chain length or coverage (*24*).

The value of τ_0 represents the adhesive contribution to friction because it gives the yield stress in the absence of an external pressure. In Fig. 2A, the interactions are purely repulsive ($r_c = 2^{1/6}$), and τ_0 is negative. Including the attractive tail of the potential and increasing ε_w increases τ_0 to positive values, but the maximum value of τ_0 that we have found for incommensurate surfaces is $\sim 0.3\varepsilon/\sigma^3$ or 12 MPa. This value is comparable to the largest value observed between mica surfaces and also to the maximum pressures accessible in these experiments (*12, 13*). The pressures in typical load-bearing contacts are much larger. In this limit, τ_0 becomes irrelevant and μ_s approaches α.

Because experiments find different μ_s for different materials, some potential parameters must change α. Figure 2B shows the effect of changing one parameter at a time from our standard set. Increasing $\varepsilon_w/\varepsilon$ from 1 to 2 produces almost no change in τ_s, but decreasing σ_w/σ from 1.0 to 0.9 increases α by 50%, and increasing this ratio to 1.5 decreases α by a factor of 6. The opposite trend is seen for d/σ, where an increase from 1.2 to 1.5 increases α to 0.073.

These trends can be understood in terms of a simple geometrical model. At the large pressures of interest, the repulsive interactions between wall atoms and monomers are dominant. Atoms and monomers cannot be closer than an effective hard sphere diameter on the order of σ_w. This diameter is very insensitive to pressure because the repulsive force rises as $\varepsilon_w(\sigma_w/r)^{13}$ as r decreases. For the same reason, changing ε_w by a factor of 2 has little effect on the system. In contrast, decreasing σ_w/d allows monomers to penetrate more deeply into the wells between wall atoms. In order to slide, monomers must move up a ramp defined by the surface of closest approach. To overcome the normal load, F_s must equal L times the maximum slope of the ramps. As σ_w/d decreases, the ramps become steeper, resulting in the increase in α seen in Fig. 2B. We have confirmed that the surfaces do indeed move apart as the yield stress is approached and that this displacement increases with α.

The values of α in Fig. 2 range from 0.008 to 0.15 and are similar to measured values for some very smooth, weakly interacting surfaces such as MoS_2 (*11*) or mica (*12*). Most unlubricated macroscopic objects exhibit μ_s of 0.1 to 0.5 and have much more complex geometries, chemistries, and third bodies. It remains to be seen how our results relate to this rich spectrum of experimental systems. One possibility is that the atomic-scale roughness present on most surfaces increases α (*16*). For example, we find $\alpha = 0.3$ at a coverage of 1/8 for surfaces made by slicing through an amorphous solid. The inclusion of grain boundaries, steps, and other defects would also affect α. Some of the increase in μ_s may be due to τ_0/P in Eq. 2. A final possibility is that more realistic models for hydrocarbon molecules and their interactions with surfaces would increase α. Some thin molecular layers are used as boundary lubricants to lower static friction, and the relation between molecular structure and the friction between incommensurate surfaces will be an interesting question for future studies.

References and Notes

1. D. Dowson, *History of Tribology* (Longman, New York, 1979).
2. F. P. Bowden and D. Tabor, *The Friction and Lubrication of Solids* (Oxford Univ. Press, Oxford, 1958).
3. G. M. McClelland and J. N. Glosli, in *Fundamentals of Friction*, H. M. Pollock and I. L. Singer, Eds. (Springer-Verlag, Berlin, 1990), pp. 405–425; G. A. Tomlinson, *Philos. Mag.* **7**, 905 (1929).
4. K. Shinjo and M. Hirano, *Surf. Sci.* **283**, 473 (1993); Y. I. Frenkel and T. Kontorova, *Zh. Eksp. Teor. Fiz.* **8**, 1340 (1938).
5. A. Volmer and T. Natterman, *Z. Phys. B* **104**, 363 (1997).
6. M. O. Robbins and E. D. Smith, *Langmuir* **12**, 4543 (1996).
7. J. H. Dieterich and B. D. Kilgore, *Pure Appl. Geophys.* **143**, 283 (1994); *Tectonophysics* **256**, 219 (1996).
8. P. Berthoud and T. Baumberger, *Proc. R. Soc. London Ser. A* **454**, 1615 (1998).
9. J. A. Greenwood and J. B. P. Williamson, *ibid.* **295**, 300 (1966).
10. B. J. Briscoe and D. J. Tabor, *J. Adhes.* **9**, 145 (1978); B. J. Briscoe and D. C. B. Evans, *Proc. R. Soc. London Ser. A* **380**, 389 (1982).
11. I. L. Singer, in *Fundamentals of Friction*, I. L. Singer and H. M. Pollock, Eds. (Elsevier, Amsterdam, 1992), pp. 237–261.
12. M. L. Gee, P. M. McGuiggan, J. N. Israelachvili, A. M. Homola, *J. Chem. Phys.* **93**, 1895 (1990); A. M. Homola, J. N. Israelachvili, P. M. McGuiggan, M. L. Gee, *Wear* **136**, 65 (1990).
13. J. V. Alsten and S. Granick, *Langmuir* **6**, 876 (1990); A. L. Demirel and S. Granick, *J. Chem. Phys.* **109**, 1 (1998).
14. J. N. Glosli and G. M. McClelland, *Phys. Rev. Lett.* **70**, 1960 (1993).
15. The interfacial interactions may be strong enough to meet this condition in special cases, such as clean metal surfaces in ultrahigh vacuum.
16. Real surfaces are rarely perfect single crystals, but including disorder without third bodies does not seem to explain experimental observations. The static friction between stiff random surfaces is a finite-size effect that drops as the inverse of the contact diameter. We find that values can be appreciable on the scale of AFM tips (<40 atomic diameters), but not in micrometer-scale contacts. Elastic deformation at large scales can yield static friction, but the values are exponentially small for weak disorder (*5*).
17. J. Krim, D. H. Solina, R. Chiarello, *Phys. Rev. Lett.* **66**, 181 (1991); C. Mak and J. Krim, *Phys. Rev. B* **58**, 5157 (1998).
18. M. Cieplak, E. D. Smith, M. O. Robbins, *Science* **265**, 1209 (1994); M. S. Tomassone, J. B. Sokoloff, A. Widom, J. Krim, *Phys. Rev. Lett.* **79**, 4798 (1997); B. N. J. Persson and A. Nitzan, *Surf. Sci.* **367**, 261 (1996).
19. M. Hirano, K. Shinjo, R. Kaneko, Y. Murata, *Phys. Rev. Lett.* **78**, 1448 (1997).
20. J. x. Martin, *Phys. Rev. B* **48**, 10583 (1993).
21. M. Schoen, C. L. Rhykerd Jr., D. J. Diestler, J. H. Cushman, *Science* **245**, 1223 (1989).
22. P. A. Thompson and M. O. Robbins, *ibid.* **250**, 792 (1990).
23. ———, G. S. Grest, *Isr. J. Chem.* **35**, 93 (1995); E. Manias, G. Hadziiaoannou, G. ten Brinke, *J. Chem. Phys.* **101**, 1721 (1994).
24. M. D. Perry and J. A. Harrison, *J. Phys. Chem. B* **101**, 1364 (1997); *Thin Solid Films* **290**, 211 (1996).
25. J. P. Gao, W. D. Luedtke, U. Landman, *Phys. Rev. Lett.* **79**, 705 (1997).
26. K. Kremer and G. S. Grest, *J. Chem. Phys.* **92**, 5057 (1990).

27. Financial support from NSF grant DMR-9634131 is gratefully acknowledged. We are also grateful to Intel for donating workstations on which these simulations were run.

16 February 1999; accepted 21 April 1999

Experimental Evidence for the Source of Excess Sulfur in Explosive Volcanic Eruptions

Hans Keppler

The amounts of sulfur released in explosive volcanic eruptions are often orders of magnitude larger than those expected to result from the degassing of the erupted SiO_2-rich magma. Experimentally measured fluid/melt partition coefficients of sulfur ranged from 47 under oxidizing conditions (where SO_2 is the dominant sulfur species in the fluid) to 468 under reducing conditions (where H_2S dominates). Therefore, a few weight percent of hydrous fluid accumulated in the top of a magma chamber may extract most of the sulfur out of the entire magma reservoir and generate sulfur excesses upon eruption.

Explosive volcanic eruptions often inject enormous amounts of sulfur dioxide into the stratosphere (*1–8*). Oxidation of SO_2 produces sulfate aerosols that can backscatter sunlight for months or even years after the eruption (*9*). Accordingly, it is believed that the release of sulfur is mainly responsible for the subsequent global cooling observed after explosive volcanic activity (*9–13*). Amounts of volcanic sulfur measured from satellites are often orders of magnitude larger than those expected to result from the degassing of the erupted silicic melt. The 1991 eruption of

Bayerisches Geoinstitut, Universität Bayreuth, 95440 Bayreuth, Germany.

Mount Pinatubo released 17 megatons of SO_2, one to two orders of magnitude more than the total amount of sulfur degassed from the erupted magma (*1–3*). Similar sulfur excesses have been observed in other recent volcanic eruptions, including Mount St. Helens 1980 (*4*), El Chichón 1982 (*5*), Nevado del Ruiz 1985 (*6*), and Redoubt 1989 (*7*). A variety of sources for excess sulfur have been proposed, including breakdown of anhydrite $CaSO_4$ (*14*), evaporation of hydrothermal systems or of precipitated sulfur near the surface (*15*), degassing of unerupted magma at depth (*16*), magma mixing (*3*), and the release of a hydrous fluid present inside the magma chamber before the eruption (*1, 2, 4, 5*). Most of these models may only be plausible under special circumstances, for example in the presence of abundant anhydrite phenocrysts in the lava or in cases where extensive hydrothermal systems existed before the eruption. Here, I tested whether small amounts of hydrous fluid in the magma chamber could extract most of the sulfur out of the entire reservoir by measuring the partition coefficient of sulfur between hydrous fluids and water-saturated SiO_2-rich silicate melts (*1*).

Little is known about the distribution of sulfur between hydrous fluids and magmas. Some attempts have been made to estimate the sulfur contents of hydrous fluid in equilibrium with silicate melt and sulfur-bearing minerals in experimental charges (*17*). These mass balance calculations suggested that under some conditions the fluid phase might be rich in sulfur, while under other conditions hardly any sulfur enters the fluid.

I performed experiments such that only hydrous fluid and silicate melt coexisted in the experimental charges. Under these conditions, fluid/melt partition coefficients can be measured with high precision. Sulfur reacts with most noble metals conventionally used as sample containers in experimental studies, such as Pt, Ag, and Pd. Therefore, I used gold as a capsule material. Test experiments showed that no measurable amount of sulfur (<1% of the charge) was lost from the gold capsules or absorbed by gold during the runs. Experiments were carried out in rapid-quench cold-seal vessels using water as a pressure medium at 0.5 to 3 kbar and 750° to 850°C. Under these conditions, gold is sufficiently permeable for hydrogen to allow control of the redox conditions in the charge by external buffers (*18*). In most experiments, the oxidation state of the charge was controlled by the intrinsic oxygen fugacity of the autoclave imposed by the reaction of the Nimonic 105 superalloy with water, which yielded an oxygen fugacity about 0.5 log units above the Ni-NiO buffer. In some experiments, an external Co-CoO buffer was used. A few experiments were also carried out with an external hematite-magnetite buffer in rapid-quench TZM-alloy bombs with argon as the pressure medium. Starting materials were solutions of H_2SO_4 in water and glasses of haplogranitic compositions (40 weight % $NaAlSi_3O_8$, 35 weight % SiO_2, and 25 weight % $KAlSi_3O_8$). After run durations between 2 and 64 days, samples were quenched to room temperature within 1 to 2 s and the quenched glasses were analyzed for sulfur by electron microprobe (*19*); 30 to 40 spots per sample were analyzed using a defocused beam and counting times of 60 s per spot. The fluid composition was determined by mass balance. Fluid/melt partition coefficients D were calculated according to $D = c_{fluid}/c_{melt}$, where c_{fluid} and c_{melt} are the concentrations (in weight percent) of sulfur in the fluid and the melt, respectively (Table 1).

Sulfur always partitions into the hydrous fluid (Fig. 1). At an oxygen fugacity 0.5 log units above the Ni-NiO buffer, D is 47 ± 4. Experiments under even more oxidizing conditions equivalent to the hematite-magnetite buffer gave virtually identical results. Under more reducing conditions equivalent to the Co-CoO buffer, D is 468 ± 32; this is an exceptionally high value for a fluid/melt partition coefficient. The strong influence of oxygen fugacity on the behavior of sulfur may be controlled by speciation. Under oxidizing conditions near the Ni-NiO buffer, sulfur is present mostly as SO_2, while H_2S dominates at the Co-CoO buffer, according to micro-Raman spectra of fluid inclusions trapped in the quenched glass. A similar change in speciation with oxygen fugacity is known to occur in

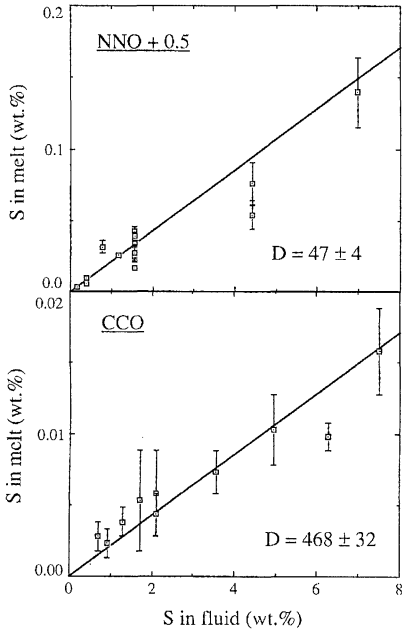

Fig. 1. Distribution of sulfur between haplogranitic melt and hydrous fluid at 2 kbar and 850°C. Oxygen fugacity in the experiments was 0.5 log units above the Ni-NiO buffer (NNO + 0.5) or equivalent to the Co-CoO buffer (CCO). Fluid/melt partition coefficients D were determined by linear regression.

Table 1. Distribution of sulfur between hydrous fluid and haplogranitic melt at 2 kbar and 850°C. Uncertainties of the fluid composition are less than 5% of the values given. The detection limit of sulfur in the quenched melt was 10 ppm. Numbers in parentheses are estimated errors in the last digits.

Experiment	Run duration (days)	S in fluid (weight %)	S in melt (weight %)
	Oxygen fugacity 0.5 log units above Ni-NiO buffer		
S 75	20	1.56	0.024 (3)
S 77	20	4.41	0.054 (10)
S 80	27	0.16	0.003 (1)
S 81	27	0.40	0.006 (2)
S 124	26	0.40	0.009 (1)
S 125	14	1.56	0.016 (1)
S 126	14	6.97	0.139 (24)
S 158	45	0.79	0.031 (4)
S 159	45	1.18	0.025 (1)
S 163	4	1.56	0.026 (2)
S 164	8	1.56	0.042 (3)
S 165	16	1.56	0.033 (4)
S 166	64	1.56	0.039 (3)
S 167	32	1.56	0.033 (2)
S 168	2	1.56	0.027 (6)
S 194	4	4.41	0.076 (15)
	Oxygen fugacity of Co-CoO buffer		
S 196	7	0.16	0.002 (1)
S 197	7	0.79	0.003 (1)
S 198	8	1.56	0.005 (3)
S 199	8	3.01	0.006 (1)
S 200	10	6.97	0.015 (3)
S 201	10	0.40	0.001 (1)
S 202	9	1.18	0.004 (3)
S 203	9	1.56	0.003 (1)
S 204	10	4.41	0.009 (2)
S 205	10	5.73	0.009 (1)

hydrous silicic melts (*20*). Relative to oxygen fugacity, pressure and temperature are less important in controlling the magnitude of the partition coefficients. In a series of experiments where oxygen fugacity was 0.5 log units above the Ni-NiO buffer, D ranged from 47 to 137 at 0.5 to 3 kbar and 750° to 850°C. Similarly, changing the alkali/aluminum ratio or adding small amounts of CaO or FeO did not change the order of magnitude of the partition coefficients. However, larger concentrations of CaO or FeO may stabilize sulfur-bearing minerals (*17*) or immiscible sulfide melts.

Explosive volcanic activity requires the presence of a free fluid phase. Under conditions slightly above the Ni-NiO buffer (with D ranging from 47 to 137), 2 weight % or less fluid in the magma chamber will be sufficient to extract half of the total mass of sulfur out of the entire magma reservoir. Because the mass of erupted magma is usually only a fraction of the total melt stored in the magma chamber (*1, 21*), it is not surprising that huge amounts of excess sulfur are observed upon eruption. Under reducing conditions, where H_2S is the major sulfur species in the fluid, the extraction of sulfur becomes even more efficient; however, such reducing conditions are probably unlikely to prevail in the subduction zone setting of most explosive volcanoes (*1–7*).

The principles outlined above can be illustrated using some data from the 1991 Mount Pinatubo eruption. The Pinatubo magma contained 60 to 90 ppm of sulfur, was relatively oxidized (between the Ni-NiO and hematite-magnetite buffers), and originated from a magma chamber with a confining pressure around 2 kbar and a temperature around 780°C (*1–3* and references therein). Accordingly, D should be close to 47. This would mean that the fluid phase in equilibrium with the hydrous melt in the magma chamber should have contained between 0.56 and 0.85 weight % SO_2. To account for the estimated 17 megatons of SO_2 released would require 8 to 25 weight % of free fluid in the erupted magma that produced 5 to 10 km^3 of pyroclastic deposits. This number appears relatively large; however, seismic evidence suggests the presence of a magma chamber containing 40 to 90 km^3 of melt below Mount Pinatubo (*21*). Relative to the entire reservoir of melt in this chamber, the free fluid phase released upon eruption would only amount to 0.9 to 3 weight %. If one assumed such a small fraction of hydrous fluid to be present in the magma chamber before eruption, a sulfur partition coefficient of 47 would imply that 30 to 59% of the total sulfur in the entire magma chamber is concentrated in the fluid, provided that the fluid has reached equilibrium with the entire reservoir. This is possible if one assumes an upward accumulation of fluid over long periods into shallower parts of the magma chamber, as suggested by Gerlach *et al.* (*1*). If the original sulfur content in the melt had been 90 ppm, the highest value found in melt inclusions (*2*), this would amount to a total mass of 5 to 24 megatons of SO_2 extracted by the fluid, consistent with the estimate of 17 megatons released upon eruption.

The calculations presented above emphasize the importance of considering the amount of sulfur stored in the entire magma chamber in estimating the sulfur released in explosive volcanism. Estimates based on the sulfur content of the erupted melt alone would severely underestimate the environmental impact of explosive volcanism in the geologic past.

References and Notes

1. T. M. Gerlach, H. R. Westrich, R. B. Symonds, in *Fire and Mud: Eruptions and Lahars of Mount Pinatubo, Philippines*, C. G. Newhall and R. S. Punongbayan, Eds. (Univ. of Washington Press, Seattle, 1996), pp. 415–433.
2. P. J. Wallace and T. M. Gerlach, *Science* **265**, 497 (1994).
3. V. Kress, *Nature* **389**, 591 (1997).
4. T. M. Gerlach and K. A. McGee, *Geophys. Res. Lett.* **21**, 2833 (1994).
5. J. F. Luhr, I. S. Carmichael, J. C. Varekamp, *J. Volcanol. Geotherm. Res.* **23**, 69 (1984).
6. H. Sigurdson, S. Carey, J. M. Palais, J. Devine, *ibid.* **41**, 127 (1990).
7. T. M. Gerlach, H. R. Westrich, T. J. Casadevall, D. L. Finnegan, *ibid.* **62**, 317 (1994).
8. G. J. S. Bluth, C. C. Schnetzler, A. J. Krueger, L. S. Walter, *Nature* **366**, 327 (1993).
9. M. P. McCormick, L. W. Thomason, C. R. Trepte, *ibid.* **373**, 399 (1995).
10. K. R. Briffa, P. D. Jones, F. H. Schweingruber, T. J. Osborn, *ibid.* **393**, 450 (1998).
11. D. M. Pyle, *ibid.*, p. 415.
12. M. R. Rampino and S. Self, *ibid.* **359**, 50 (1992).
13. S. Bekki *et al.*, *Geophys. Res. Lett.* **23**, 2669 (1996).
14. J. D. Devine, H. Sigurdsson, A. N. Davis, S. Self, *J. Geophys. Res.* **89**, 6309 (1994).
15. C. Oppenheimer, *Geophys. Res. Lett.* **23**, 2057 (1996).
16. S. N. Williams *et al.*, *J. Volcanol. Geotherm. Res.* **42**, 53 (1990).
17. B. Scaillet, B. Clemente, B. W. Evans, M. Pichavant, *J. Geophys. Res.* **103**, 23937 (1998).
18. I. M. Chou, *Am. J. Sci.* **286**, 638 (1986).
19. Cameca SX 50 with operating conditions of 20 KV acceleration voltage, 50 nA beam current, ZnS and $BaSO_4$ standard.
20. M. R. Carroll and M. J. Rutherford, *Am. Mineral.* **73**, 845 (1988).
21. J. Mori, D. Eberhart-Phillips, D. Harlow, *Eos* **74** (fall meeting suppl.), 667 (1993).

22. I thank D. Krausse for carrying out all microprobe analyses presented in this study, A. Dietel and S. Lauterbach for analyses by inductively coupled plasma atomic emission spectrometry, and H. Schulze for sample preparation. I. Kravchuk performed some preliminary, unpublished experiments related to this study. Supported by the German Science Foundation (DFG) priority program on element partitioning.

20 January 1999; accepted 19 April 1999

A Mid-European Decadal Isotope-Climate Record from 15,500 to 5000 Years B.P.

Ulrich von Grafenstein,[1*] Helmut Erlenkeuser,[2] Achim Brauer,[3] Jean Jouzel,[1] Sigfus J. Johnsen[4]

Oxygen-isotope ratios of precipitation ($\delta^{18}O_p$) inferred from deep-lake ostracods from the Ammersee (southern Germany) provide a climate record with decadal resolution. The record in detail shows many of the rapid climate shifts seen in central Greenland ice cores between 15,000 and 5000 years before the present (B.P.). Negative excursions in the estimated $\delta^{18}O_p$ from both of these records likely reflect short weakenings of the thermohaline circulation caused by episodic discharges of continental freshwater into the North Atlantic. Deviating millennial-scale trends, however, indicate that climate gradients between Europe and Greenland changed systematically, reflecting a gradual rearrangement of North Atlantic circulation during deglaciation.

The Greenland ice cores show strong quasi-periodic climatic oscillations during the longer term interglacial-glacial and glacial-interglacial transitions. These Dansgaard-Oeschger events (DOEs) (*1*) are characterized by rapid warmings of almost glacial-interglacial amplitudes within decades, followed by some 2000 to 3000 years of gradual cooling, and a final cold phase of about 1000 years' duration, often with a weak, positive internal trend. Similar features have been found for Europe in long continental records of vegetation and magnetic sediment properties (*2*), as well as in marine proxy records (*3*). Modeling studies and data provide support for two alternative mechanisms: (i) triggering by oscillations of the northern hemispheric ice sheets (*3*) or (ii) oceanic oscillations without

[1]Laboratoire des Sciences du Climat et de l'Environnement (LSCE), F-91198 Gif-sur-Yvette, France. [2]Leibniz-Labor für Altersbestimmung und Isotopenforschung der Universität Kiel, Germany. [3]Laboratoire de Botanique Historique et Palynologie, Faculte des Sciences et Techniques de Saint-Jerome, Marseille, France, and GeoForschungsZentrum Potsdam, Germany. [4]Department of Geophysics, University of Copenhagen, Copenhagen, Denmark, and Science Institute, University of Iceland, Reykjavik, Iceland.

*To whom correspondence should be addressed. E-mail: uligraf@lsce.cnrs-gif.fr